



HAL
open science

Photoionization and Dissociative Photoionization of Acetaldehyde in the 10.0–13.7 eV Range by Synchrotron Photoelectron Photoion Coincidence Spectroscopy

Xiangkun Wu, Cuihong Zhang, Xuejun Gu, Christa Fittschen, Jean-christophe Loison, Madhusree Roy Chowdhury, Gustavo Garcia, Laurent Nahon, Xiaofeng Tang

► **To cite this version:**

Xiangkun Wu, Cuihong Zhang, Xuejun Gu, Christa Fittschen, Jean-christophe Loison, et al.. Photoionization and Dissociative Photoionization of Acetaldehyde in the 10.0–13.7 eV Range by Synchrotron Photoelectron Photoion Coincidence Spectroscopy. *ChemPhysChem*, 2024, 25 (13), 10.1002/cphc.202400208 . hal-04781925

HAL Id: hal-04781925

<https://hal.science/hal-04781925v1>

Submitted on 16 Nov 2024

HAL is a multi-disciplinary open access archive for the deposit and dissemination of scientific research documents, whether they are published or not. The documents may come from teaching and research institutions in France or abroad, or from public or private research centers.

L'archive ouverte pluridisciplinaire **HAL**, est destinée au dépôt et à la diffusion de documents scientifiques de niveau recherche, publiés ou non, émanant des établissements d'enseignement et de recherche français ou étrangers, des laboratoires publics ou privés.

Photoionization and dissociative photoionization of acetaldehyde in the 10.0-13.7 eV range by synchrotron photoelectron photoion coincidence spectroscopy

Xiangkun Wu,¹ Cuihong Zhang,^{1,2} Xuejun Gu,¹ Christa Fittschen,² Jean-Christophe Loison,³ Gustavo A. Garcia,⁴ Laurent Nahon,⁴ and Xiaofeng Tang¹

¹ Anhui Institute of Optics and Fine Mechanics, Hefei Institutes of Physical Sciences, Chinese Academy of Sciences, Hefei, 230031 Anhui, China

² University Lille, CNRS, UMR 8522, PC2A – Physicochimie des Processus de Combustion et de l'Atmosphère, F-59000 Lille, France.

³ Institut des Sciences Moléculaires (ISM), CNRS, Univ. Bordeaux, 351 cours de la Libération, 33400 Talence, France.

⁴ Synchrotron SOLEIL, L'Orme des Merisiers, St. Aubin, BP 48, 91192 Gif sur Yvette, France

Abstract: Photoionization and dissociative photoionization of acetaldehyde (CH_3CHO) in the 10.0–13.7 eV energy range are studied by using synchrotron radiation double imaging photoelectron photoion coincidence spectroscopy ($i^2\text{PEPICO}$). The X^2A' and A^2A'' electronic states of CH_3CHO^+ as well as the Franck-Condon gap region have been populated with several vibrational sequences and assigned in the high-resolution slow photoelectron spectrum (SPES). The adiabatic ionization energies (AIEs) of the X^2A' and A^2A'' states are measured at 10.228 ± 0.005 and 12.52 ± 0.05 eV, respectively. The present results show that the X^2A' state is a stable state while the A^2A'' state is fully dissociative to produce CH_3CO^+ , CHO^+ and CH_4^+ fragment ions. The adiabatic appearance energies (AP_{0K}) of the fragment ions are also determined through the modeling of the breakdown diagram, i.e., $\text{AP}_{0K}(\text{CH}_3\text{CO}^+) = 10.89 \pm 0.02$ eV, $\text{AP}_{0K}(\text{CHO}^+) = 11.54 \pm 0.05$ eV and $\text{AP}_{0K}(\text{CH}_4^+) = 12.37 \pm 0.05$ eV. In addition, the dissociation mechanisms of CH_3CHO^+ including statistical dissociation, direct bond breaking and isomerization are discussed with the support of theoretical potential energy surfaces.

1. Introduction

Acetaldehyde (CH_3CHO) is an oxygenated volatile organic compound significantly found in a variety of interstellar conditions¹⁻⁴ and in the Earth's atmosphere^{5,6} and whose photochemistry plays an essential role in these environments. In interstellar spaces or in the Earth's upper atmosphere, CH_3CHO has the ability to absorb vacuum ultraviolet (VUV) radiations, and therefore photoionization and dissociative photoionization are of fundamental interest, attracting attention in the past decades. Briefly, the valence-shell electronic configuration of CH_3CHO in the X^1A' ground state is expressed as $(6a')^2(7a')^2(1a'')^2(8a')^2(9a')^2(2a'')^2(10a')^2$,⁷ and CH_3CHO^+ cations can be formed in the X^2A' , A^2A'' and B^2A' electronic states after removing an electron from the outer orbitals, *i.e.*, $10a'$, $2a''$ and $9a'$. The energetics and structures of CH_3CHO^+ cations in the low-lying electronic states have been studied using various methods such as VUV absorption spectroscopy,^{8,9} electron impact ionization mass spectrometry,¹⁰ photoionization mass spectrometry,¹¹⁻¹³ photoelectron spectroscopy (PES),¹⁴⁻¹⁹ and quantum chemistry calculations.^{7,20} The vibrational structures of the X^2A' and A^2A'' electronic states were observed in the PES and have been roughly assigned with the neutral vibrational frequencies.^{14,19}

With the increment of internal energy, CH_3CHO^+ cations will dissociate and the fragmentation processes have been studied by the methods of photoionization mass spectrometry,¹³ electron ionization yield curves,^{21,22} and velocity map ion imaging.²³ The appearance energies (APs) of fragment ions in the dissociation of CH_3CHO^+ were reported at $\text{AP}(\text{CH}_3\text{CO}^+) = 10.90$ eV, $\text{AP}(\text{HCO}^+) = 12.03$ eV and $\text{AP}(\text{CH}_4^+) = 12.61$ eV,¹³ slightly above their thermodynamic thresholds. Photoelectron photoion coincidence spectroscopy (PEPICO) have also been performed to study internal energy-selected dissociation of CH_3CHO^+ . For example, Bombach et al. employed PEPICO to measure the relative ratios of CH_3CHO^+ , CH_3CO^+ , CHO^+ and CH_3^+ and found no state-specific fragmentation behaviors in the dissociation.²⁴ Johnson et al. utilized PEPICO to explore dissociation of excited states of CH_3CHO^+ ,²⁵ and found that the formation of the CH_4^+ fragment ion from the A^2A'' state has state-specific behavior. PEPICO measurements provide an overall picture for the dissociation of CH_3CHO^+ . But

previous PEPICO experiments usually used fixed photon energy He I or He II lamps as photoionization light source, and the dissociative information in the Franck-Condon gap region is very limited. The accurate appearance energies of fragment ions are still needed to be measured, in particular some of them lying in the Franck-Condon gap region.

In this study, photoionization and dissociative photoionization of CH₃CHO in the 10.0-13.7 eV energy range have been studied in detail by using the method of double imaging photoelectron photoion coincidence spectroscopy (i²PEPICO) coupled with modern tunable VUV synchrotron radiation as photoionization light source. The X²A' and A²A" electronic states of CH₃CHO⁺ cations as well as the Franck-Condon gap region between these two states have been prepared and studied. The high-resolution slow photoelectron spectrum (SPES) has been acquired and shows vibrational structures that are assigned *via* theoretical calculations that include a Franck-Condon simulation. CH₃CO⁺, CHO⁺ and CH₄⁺ fragment ions are observed in the photoionization mass spectra and their individual adiabatic appearance energies have been precisely determined by modeling the breakdown diagram using a statistical theory. In addition, dissociation mechanisms corresponding to each fragment ion have been discussed with the aid of theoretical potential energy surfaces.

2. Experimental and Computational Methods

The experiments were performed on the DESIRS VUV beamline at synchrotron SOLEIL, the French national synchrotron facility, by using the i²PEPICO spectrometer DELICIOUS III. The configurations of the synchrotron beamline²⁶ and the i²PEPICO spectrometer²⁷ have already been introduced in detail in our previous work so that only a short description is presented here. Briefly, horizontally polarized synchrotron photons emitted from an undulator were dispersed with a 6.65 m normal incidence monochromator equipped with a 200 lines·mm⁻¹ grating, providing an energy resolution of ~ 3 meV. A gas filter located upstream of the beamline and presently filled with krypton gas was used to suppress higher-order harmonics photons from the undulator. A photodiode was installed to measure the photon flux to normalize signals

during the photon energy scans.

CH₃CHO evaporated from a bubbler cooled at 3°C was mixed with helium carrier gas in a flow tube with a total pressure at 0.2 mbar. After passing through two skimmers (1 mm and 2 mm diameter), the gas beam from the flow tube crossed the synchrotron photon beam at the center of the i²PEPICO spectrometer, which is composed of an electron velocity map imaging (VMI) device and a modified Wiley-McLaren 3D ion momentum imaging analyzer. Electrons and ions formed by photoionization were extracted in opposite directions by a constant electric field, and two delay-line based position-sensitive detectors with 80 and 40 mm diameters, respectively, were installed at the end of the electron and ion flight tubes to record their signals. The electron images were mass-filtered by coincidence with a given ion and Abel inverted. The resulting coincidence signal as a function of electron and photon energy was further treated to obtain SPES or mass-selected SPES.²⁸

The statistical modeling program, miniPEPICO, was employed to model the breakdown diagram.²⁹ Briefly, the program accounts for both the internal energy distribution of the parent molecule, which would otherwise redshift the observed appearance energy, and for kinetic effects which would lead to a blue shift. For thermal effects, the internal energy distribution is calculated assuming that all vibrational modes are thermalized to a temperature that is adjusted to fit the experimental breakdown diagram. A direct state counting algorithm is used to obtain the density of states of the parent from a given set of vibrational modes and rotational constants which is weighted by a Boltzmann distribution to yield the internal energy distribution. The vibrational frequencies and rotational constants were obtained from the optimized structures at the B3LYP/6-311++G(d,p) level of theory. If the parent ion is metastable within the experimental analysis time (a few μsec here) or the fragments are competing, kinetic effects are considered for which the dissociation rate constant as a function of internal energy needs to be calculated according to the Rice–Ramsperger–Kassel–Marcus (RRKM) theory with the formula (1),³⁰⁻³²

$$k(E) = \frac{\sigma \cdot N^\ddagger(E - AP_0K)}{h \cdot \rho(E)}, \quad (1)$$

in which σ corresponds to the symmetry of the reaction coordinate, $N^\ddagger(E - AP_{0K})$ is the state number of the transition state with an excess energy $E - AP_{0K}$, AP_{0K} is the 0 K appearance energy, h is Planck's constant, and $\rho(E)$ is the density of states of the precursor. AP_{0K} was adjusted as well as the entropy of the transition state, the latter by varying the frequencies of the transitional modes to obtain the best fit of the breakdown diagram.

Quantum chemical calculations were performed to get the theoretical potential energy surface of dissociation by using the Gaussian 16 A.03 program package.³³ The geometries of the neutral, the parent ion, the fragment ions and the transition states in the ground state were optimized using the density functional theory (DFT). The structures of the excited states were optimized by the time-dependent density functional theory (TD-DFT). The calculations were done at the B3LYP/6-311++G(d,p) level of theory.³⁴ The energies of the stationary points at the potential energy surface were checked by frequency analysis and further refined using the Gaussian-4 (G4) theory.³⁵

The Franck-Condon (FC) factors were obtained within the double harmonic approximation including the Duschinsky rotation, as implemented in the Gaussian program package with the same level of theory as above. The FC factors were then convolved with a Gaussian function of 80 cm^{-1} full width at half-maximum (FWHM) to get the simulated PES, after scaling down the vibrational frequencies by a 0.963 factor, as indicated for the B3LYP/6-311++G(d,p) level of theory.³⁶

3. Results and discussion

3.1 Slow photoelectron spectra

The SPES of CH_3CHO in the 10.0–13.7 eV energy range was measured by scanning the synchrotron photon energy with a step size of 12 meV and is presented in Figure 1(a). Within this energy range, the two lowest lying electronic states of CH_3CHO^+ , X^2A' and A^2A'' , can be accessed and show vibrational structures that have been previously reported and assigned,^{19, 20, 23} albeit using the vibrational frequencies of the neutral molecule.^{14, 19} Note that upon ionization, the structures of the neutral molecule and its cation as well as their vibrational frequencies are different, and thus a

detailed assignment of these peaks in the SPES is still necessary. In addition, unlike previous PES acquired with He I/II light sources,^{15, 22, 23} in the SPES of Figure 1(a) some weak signals can be discerned in the Franck-Condon gap region between the X^2A' and A^2A'' states, mainly from autoionization of neutral Rydberg states populated in the photon energy scan. This is especially evident in the mass-selected SPES of m/z 43 (see Figure 1(b), which is perhaps why Yenchu et al. (Ref 19) did not discuss the FC gap region in their reported total threshold PES (TPES).

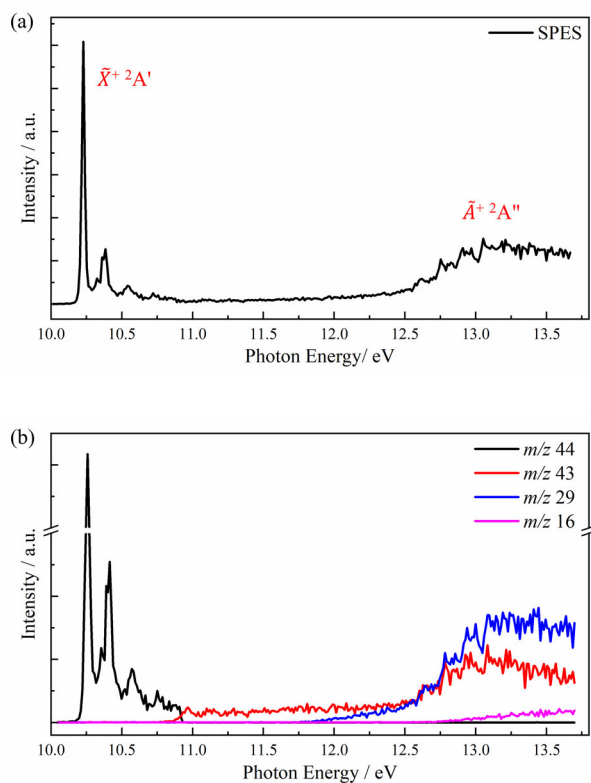


Figure 1. (a) Slow photoelectron spectrum of acetaldehyde and (b) mass-selected slow photoelectron spectra corresponding to the parent and fragment ions in the 10.00–13.70 eV energy range.

For clarity, the SPES in 10.1–11.00 eV X^2A' energy range is expanded and presented in Figure 2(a), as well as the simulated PES. Based on the simulation, the strongest peak at 10.228 ± 0.005 eV is attributed to the adiabatic transition of $X^1A' \rightarrow X^2A'$, agreeing very well with the calculated AIE of CH_3CHO at 10.226 eV using the G4 method. The present AIE is also consistent with previous results of the Rydberg-series analyses (10.2293 ± 0.0007 eV) and threshold photoelectron spectroscopy

(10.228 ± 0.01 eV).

In Figure 2(a), the peak at 10.325 eV (780 cm⁻¹ above the 0₀⁰ peak) is attributed to a ν_2 overtone of CH₃CHO⁺, as confirmed by the FC simulation, indicating a frequency of ν_2 at 390 cm⁻¹. Note that previous works attributed this transition to either the C-C=O bend, ν_{10} , or CH₃ rock, ν_9 .^{14, 19} Our theoretical calculations show that the ν_2 vibration corresponds to the C-C-O bending of CH₃CHO⁺ with a frequency of 363 cm⁻¹. Another intense peak at 10.361 eV (1070 cm⁻¹ above the 0₀⁰ peak) in the SPES arises from the 7₀¹ vibrational transition, and the partially overlapped peak at 10.385 eV (1264 cm⁻¹ above the 0₀⁰ peak) comes from the 8₀¹ vibrational transition. These two vibrational modes correspond to the C-H rocking and the CH₃ umbrella of CH₃CHO⁺, with their calculated frequencies at 1106 and 1259 cm⁻¹, respectively. In addition, another two peaks at 10.493 and 10.517 eV are assigned as the 5₀¹7₀¹ and 7₀¹8₀¹ combination bands, respectively. The displacement vectors of the ν_2 , ν_7 and ν_8 vibrational modes as well as their calculated frequencies are illustrated in Figure 2(b).

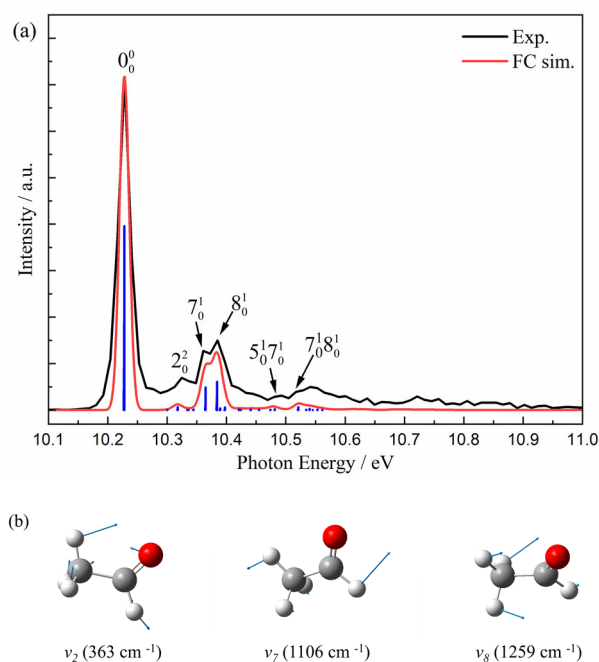


Figure 2. (a) Expanded slow photoelectron spectrum of acetaldehyde in the 10.1–11.0 eV energy range and corresponding simulation with the FC factors in blue. (b) Displacement vectors of the three most intense vibrational modes of the X²A' cationic ground state.

The expanded SPES of the A²A" state in the 12.3–13.7 eV energy range is

presented in Figure 3(a). Complex vibrational structures can be observed in this energy region which are well reproduced by the FC simulation, showing that experimental vibronic bands are made up of several and even numerous individual transitions. The FC simulation shows a weak 0_0^0 transition for $X^1A' \rightarrow A^2A''$ located at 12.516 ± 0.05 eV, which low intensity is the consequence of a large geometric change upon photoionization. According to the simulation, the SPES of the A^2A'' state mainly exhibits ν_6 and ν_8 vibrational excitations, as well as combination bands such as $\nu_6\nu_8$, $\nu_6\nu_{11}$ and $\nu_6\nu_{13}$. The fundamental displacement vectors of the ν_6 , ν_8 , ν_{11} and ν_{13} vibrational modes as well as their calculated frequencies are shown in Figure 3 (b).

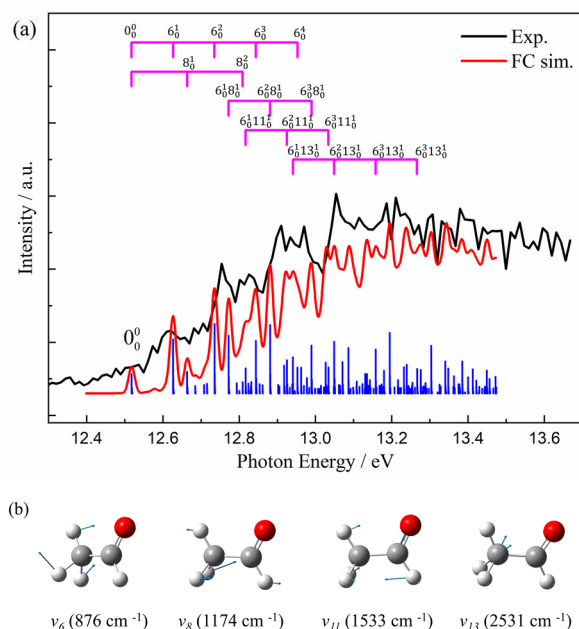


Figure 3. (a) Expanded slow photoelectron spectrum of acetaldehyde in the 12.35–13.70 eV energy range and its simulated results with the FC factors in blue. (b) Displacement vectors of the four most intense vibrational modes of the A^2A'' cationic electronic state.

3.2 Photoionization mass spectra

Photoionization mass spectra of acetaldehyde were measured and the mass spectra matrix—coincidence signal as a function of mass and photon energy—in the 10.0–13.7 eV energy range is presented in Figure 4, as well as the integrated mass spectrum. The most intense peak at m/z 44 is attributed to the parent ion CH_3CHO^+ , the peak at m/z 43 to the fragment ion CH_3CO^+ from the H loss channel of CH_3CHO^+ , the peak at m/z 29 to the fragment ion CHO^+ from the CH_3 loss channel, and the minor peak at m/z 16 to

the fragment ion CH_4^+ . The matrix clearly shows that the appearance energies of these fragment ions are different. In addition, due to the released kinetic energy in the dissociation, the peak widths of the fragment ions increase with photon energy and are wider than that of the parent ion.

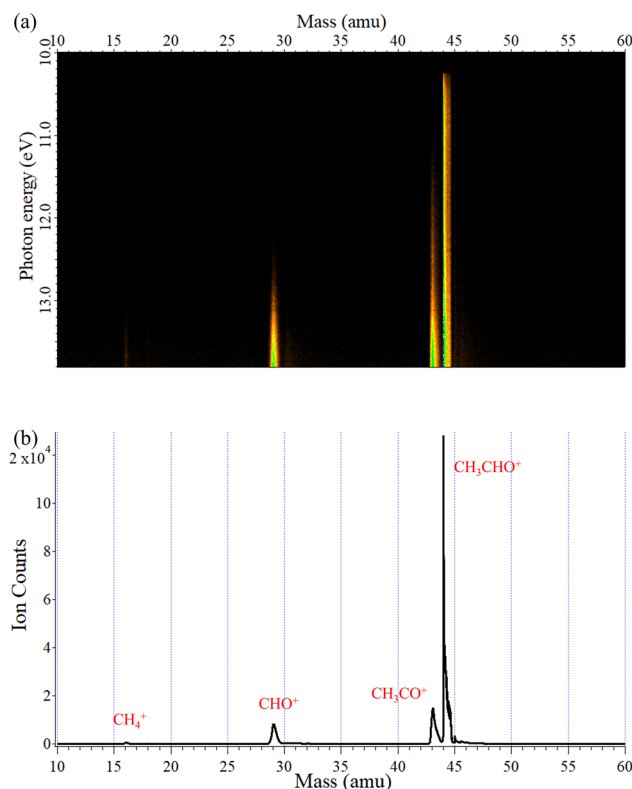


Figure 4. (a) Photoionization mass spectra matrix of acetaldehyde in the 10.0–13.7 eV energy range and (b) their integrated mass spectrum.

Mass-selected SPES corresponding to each of the detected mass channels ($m/z = 44, 43, 29, 16$) are illustrated in Figure 1 (b). Within the energy range of the X^2A' state, the mass-selected SPES of CH_3CHO^+ ($m/z 44$) is very similar to the SPES in Figure 1(a), indicating that the X^2A' ground state is a stable state. With the increase of photon energy, the parent ion CH_3CHO^+ disappears in the mass-selected SPES and dissociates into several fragment ions. Among the three fragment ions, CH_3CO^+ ($m/z 43$) has the lowest appearance energy which, interestingly, falls within the FC gap region, in accordance with the disappearance of the parent ion. As shown in the mass-selected SPES of $m/z 29$, the fragment ion HCO^+ also first appears in the Franck-Condon gap region and becomes the major fragment ion in the energy range of the A^2A'' state. The

A²A" state is a fully dissociative state and the appearance of the minor fragment ion CH₄⁺ lies in the A²A" state.

3.3 Breakdown diagram and dissociative ionization mechanism

The breakdown diagram, *i.e.*, the molar fraction of the parent and different fragment as a function of deposited energy (which equals the photon energy for events correlated with threshold electrons), is obtained from the mass-selected SPES and presented in Figure 5. The breakdown diagram shows that, with the disappearance of the parent ion CH₃CHO⁺, the fraction of CH₃CO⁺ increases with photon energy and reaches an abundance of 100%. Further increasing the photon energy opens a parallel channel to the HCO⁺ formation, which dominates above 12.7 eV. The emergence of the minor fragment ion CH₄⁺ lies at around 12.60 eV and must come from a third parallel dissociation channel, as neither CH₃CO⁺ nor HCO⁺ can produce CH₄⁺.

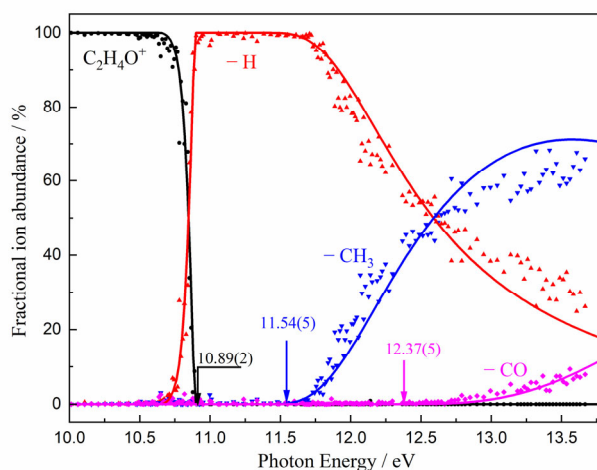


Figure 5. Breakdown diagram of acetaldehyde in the 10.00–13.70 eV energy range. Dots and triangles represent the experimental fractional abundances, and solid lines show the simulated breakdown curves.

To rationalize the dissociation mechanisms of CH₃CHO⁺, the potential energy surface the energies of the dissociation limits and transition states involving multiple bond-breaking and isomerization pathways have been calculated and are presented in Figure 6. Theoretical calculations show that the lowest-energy dissociation channel leading to the CH₃CO⁺ (*m/z* 43) + H fragments is reached through a 0.19 eV reverse barrier with a loose transition state [2][‡] at 10.96 eV (0.73 eV above the parent ion [1]), and results in a linear C–C=O geometry for CH₃CO⁺. The formation of the CH₂CHO⁺

fragment (not shown in Fig. 6) is not expected, first because it has a much higher barrier of 2.97 eV relative to [1], which is out of the present energy range and second it would not compete with the hydrogen loss of the aldehyde group (formation of CH_2CO^+). The C–C bond breaking of CH_3CHO^+ can directly form the fragment ion HCO^+ [4] at 11.71 eV (1.48 eV above the parent ion), without barrier or transition state, which is why this channel becomes dominant over [3] once it is energetically accessible. The CO-loss channel involves a hydrogen atom transfer from the aldehyde group to the methyl group and then yields CH_4^+ [6] via the transition state [5][‡] with a 2.62 eV barrier.

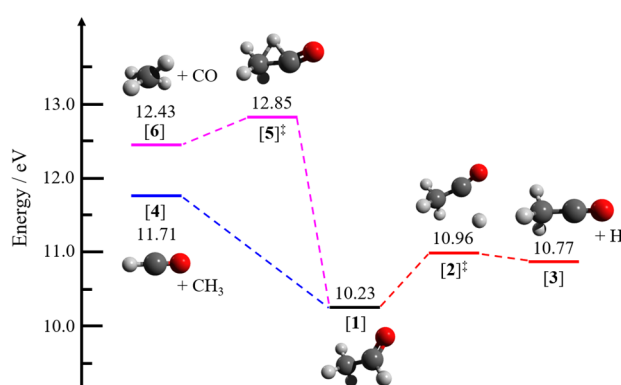


Figure 6. Energy diagram of the dissociation of the acetaldehyde cation. Energies are relative to the most stable neutral *para*-anisaldehyde conformer and calculated with the G4 method.

Obtaining precise thermochemical values from the experimental breakdown curves is not trivial because, as mentioned above, thermal and kinetic effects need to be considered. Therefore, based on the calculated energy diagram, a statistical decomposition model was constructed to reproduce the breakdown curves in order to extract the 0K appearance energies of the three channels involved, as shown in Figure 5. For the lowest-energy decomposition channel, responsible for the hydrogen atom loss, the $\text{AP}_{0\text{K}}(\text{CH}_3\text{CO}^+)$ is determined at 10.89 ± 0.02 eV, agreeing well with the theoretically predicted energy of [2][‡] at 10.96 eV. In parallel with the decrease of the H loss channel, the fraction of the HCO^+ fragment ion increases quickly since the H_2 loss is kinetically more favorable than the H loss. According to the statistical model, the $\text{AP}_{0\text{K}}(\text{CHO}^+)$ is measured at 11.54 ± 0.05 eV, slightly below the calculated value of 11.71 eV for the direct bond breaking channel. The CH_4^+ fragment ion exhibits a gradual increase above the threshold energy, implying kinetically favored

fragmentation. Interestingly, although the $AP_{0K}(CH_4^+) = 12.37 \pm 0.05$ eV extracted from the model agrees well with the 12.43 eV value from the G4 calculation and the 12.32 eV from the Active Thermochemical Tables (ATcT),³⁷ it appears 0.48 eV lower than the calculated energy of the transition state $[5]^\ddagger$, suggesting another mechanism in play.

4. Conclusions

We have studied the VUV photoionization and dissociative photoionization of acetaldehyde in the energy range of 10.0-13.7 eV using *i*²PEPICO and synchrotron radiation. Mass-selected SPES have been acquired and the vibrational structures observed in the X^2A' and A^2A'' electronic states have been assigned with the help of theoretical calculations and a FC simulation, showing that mainly the ν_2 , ν_7 and ν_8 vibrational modes are active in transitions to the X^2A' state. Vibronic transitions to the A^2A'' state are more numerous due to the larger geometry changes upon ionization, nevertheless the ν_6 , ν_8 , $\nu_6\nu_8$, $\nu_6\nu_{11}$ and $\nu_6\nu_{13}$ vibrational levels have been identified. The AIEs of the X^2A' and A^2A'' states are determined at 10.228 ± 0.005 and 12.52 ± 0.05 eV, respectively.

Both the parent ion (CH_3CHO^+) and the fragment ions (CH_3CO^+ , HCO^+ and CH_4^+) are observed in the photoionization mass spectra within the present energy range. The X^2A' ground state is bound while the A^2A'' electronic state is fully dissociative. Three parallel channels with the H, CH_3 and CO loss lead to the formation of CH_3CO^+ (m/z 43), CHO^+ (m/z 29) and CH_4^+ (m/z 16) fragment ions, respectively. The adiabatic appearance energies of the fragment ions, $AP_{0K}(CH_3CO^+) = 10.89 \pm 0.02$ eV, $AP_{0K}(CHO^+) = 11.54 \pm 0.05$ eV and $AP_{0K}(CH_4^+) = 12.37 \pm 0.05$ eV, are determined from statistical modeling of the breakdown diagram. Moreover, the dissociation mechanisms of CH_3CHO^+ including statistical dissociation, direct bond breaking and isomerization have also been revealed with the aid of the calculated dissociation limits and transition state energies.

Author contributions

Xiangkun Wu: formal analysis, writing – original draft; Cuihong Zhang: investigation; Xuejun Gu: investigation; Christa Fittschen: investigation; Jean-

Christophe Loison: investigation; Gustavo A. Garcia: methodology, data curation, investigation, and writing – review and editing; Laurent Nahon: methodology, investigation, and writing – review and editing; Xiaofeng Tang: conceptualization, methodology, project administration, writing – original draft, and writing – review and editing.

Conflicts of interest

The authors have no conflicts to declare.

Acknowledgments

This work was supported by the National Natural Science Foundation of China (No. 42120104007), the HFIPS Director's Fund (No. YZJJ202401-CX) and the Cai Yuanpei Project (No 50892QC). C. F. would like to thank the support from the Chinese Academy of Sciences President's International Fellowship Initiative (No. 2018VMA0055). The authors acknowledge the SOLEIL general staff for smoothly running the facility and providing synchrotron beamtime under the proposal 20210072. The project has received financial support from the French Agence Nationale de la Recherche (ANR), under contract ANR-21-CE29-0017 (ZEPHIRS).

References

- [1] S. Cazaux, A. G. G. M. Tielens, C. Ceccarelli, A. Castets, V. Wakelam, E. Caux, B. Parise, D. Teyssier, *Astrophys. J.*, **2003**, 593, L51.
- [2] J. Crovisier, D. Bockelée-Morvan, P. Colom, N. Biver, D. Despois, D. C. Lis, *Astron. Astrophys.*, **2004**, 418, 1141.
- [3] M. A. Requena-Torres, J. Martín-Pintado, A. Rodríguez-Franco, S. Martín, N. J. Rodríguez-Fernández, P. de Vicente, *Astron. Astrophys.*, **2006**, 455, 971-985.
- [4] A. A. Jaber, C. Ceccarelli, C. Kahane, E. Caux, *Astrophys. J.*, **2014**, 791, 29.
- [5] R. S. Hornbrook, A. J. Hills, D. D. Riemer, A. Abdelhamid, F. M. Flocke, S. R. Hall, L. G. Huey, D. J. Knapp, J. Liao, R. L. Mauldin III, et al., *J. Geophys. Res.: Atmos.*, **2016**, 121, 9789.
- [6] T. K. Koenig, R. Volkamer, S. Baidar, B. Dix, S. Wang, D. C. Anderson, R. J. Salawitch, P. A. Wales, C. A. Cuevas, R. P. Fernandez, et al., *Atmos. Chem. Phys.* **2017**, 17, 15245.
- [7] M. Vinodkumar, C. Limbachiya, H. Desai, P. C. Vinodkumar, *RSC Adv.*, **2015**, 5, 69466.
- [8] A. D. Walsh, *Proc. R. Soc. Lond., Ser. A*, **1946**, 185, 176.
- [9] H. Ogata, J. Kitayama, M. Koto, S. Kojima, Y. Nihei, H. Kamada, *Bull. Chem. Soc. Jpn.*, **1974**, 47, 958.
- [10] K. N. Walzl, C. F. Koerting, A. Kuppermann, *J. Chem. Phys.*, **1987**, 87, 3796.
- [11] H. Hurzeler, M. G. Inghram, J. Morrison, *J. Chem. Phys.*, **1958**, 28, 76.

- [12] P. Warneck, *Z. Naturforsch. A*, **1974**, *29*, 350.
- [13] H. Jochims, W. Lohr, H. Baumgärtel, *Chem. Phys. Lett.*, **1978**, *54*, 594.
- [14] D. Chadwick, A. Katrib, *J. Electron Spectrosc. Relat. Phenom.*, **1974**, *3*, 39.
- [15] W.-C. Tam, D. Yee, C. Brion, *J. Electron Spectrosc. Relat. Phenom.*, **1974**, *4*, 77.
- [16] K. Kimura, S. Katsumata, T. Yamazaki, H. Wakabayashi, *J. Electron Spectrosc. Relat. Phenom.*, **1975**, *6*, 41.
- [17] S. McGlynn, J. Meeks, *J. Electron Spectrosc. Relat. Phenom.*, **1975**, *6*, 269.
- [18] R. Hernandez, P. Masclet, G. Mouvier, *J. Electron Spectrosc. Relat. Phenom.*, **1977**, *10*, 333.
- [19] A. J. Yench, M. R. Siggel-King, G. C. King, A. E. Malins, M. Eypper, *J. Electron Spectrosc. Relat. Phenom.*, **2013**, *187*, 65.
- [20] V. J. Rani, A. K. Kanakati, S. Mahapatra, *J. Phys. Chem. A*, **2022**, *126*, 6581.
- [21] T. M. El-Sherbini, S. Allam, M. Migahed, A. Dawoud, *Z. Naturforsch. A*, **1981**, *36*, 1334.
- [22] K. Głuch, J. Cytawa, L. Michalak, *Int. J. Mass Spectrom.*, **2008**, *273*, 20.
- [23] K. M. Kapnas, L. M. McCaslin, C. Murray, *Phys. Chem. Chem. Phys.*, **2019**, *21*, 14214.
- [24] R. Bombach, J.-P. Stadelmann, J. Vogt, *Chem. Phys.*, **1981**, *60*, 293.
- [25] K. Johnson, I. Powis, C. Danby, *Chem. Phys.*, **1982**, *70*, 329.
- [26] L. Nahon, N. de Oliveira, G. A. Garcia, J.-F. Gil, B. Pilette, O. Marcouillé, B. Lagarde, F. Polack, *J. Synchrotron Radiat.*, **2012**, *19*, 508.
- [27] G. Garcia, B. Cunha de Miranda, M. Tia, S. Daly, L. Nahon, *Rev. Sci. Instrum.*, **2013**, *84*.
- [28] G. A. Garcia, L. Nahon, I. Powis, *Rev. Sci. Instrum.*, **2004**, *75*, 4989.
- [29] B. Sztáray, A. Bodi, T. Baer, *J. Mass Spectrom.*, **2010**, *45*, 1233.
- [30] O. K. Rice, H. C. Ramsperger, *J. Am. Chem. Soc.*, **1927**, *49*, 1617.
- [31] O. K. Rice, H. C. Ramsperger, *J. Am. Chem. Soc.*, **1928**, *50*, 617.
- [32] R. A. Marcus, O. Rice, *J. Phys. Chem.*, **1951**, *55*, 894.
- [33] M. J. Frisch, G. W. Trucks, H. B. Schlegel, G. E. Scuseria, M. A. Robb, J. R. Cheeseman, G. Scalmani, V. Barone, G. A. Petersson, H. Nakatsuji *Gaussian16 (Revision A. 03)*. **2016**.
- [34] E. De Castro, F. Jorge, *J. Chem. Phys.*, **1998**, *108*, 5225
- [35] L. A. Curtiss, P. C. Redfern, K. Raghavachari, *J. Chem. Phys.*, **2007**, *126*.
- [36] D. O. Kashinski, G. M. Chase, R. G. Nelson, O. E. Di Nallo, A. N. Scales, D. L. VanderLey, E. F. C. Byrd, *J. Phys. Chem. A*, **2017**, *121*, 2265.
- [37] B. Ruscic, D. Bross, Active Thermochemical Tables (ATcT) values based on ver. TN 1.130 of the Thermochemical Network, *available at ATcT. anl. gov.*, **2023 Nov. access**.

Table Of Contents

